Rotational Dynamics of HCN−M (M = Na, K, Rb, Cs) van der Waals Complexes Formed on the Surface of Helium Nanodroplets†

Gary E. Douberly*,‡ and Roger E. Miller§

Department of Chemistry, The University of North Carolina at Chapel Hill, Chapel Hill, North Carolina 27599-3290

Received: January 3, 2007; In Final Form: May 25, 2007

Infrared laser spectroscopy was used to probe the unique rotational dynamics of the HCN−M (M = Na, K, Rb, Cs) complexes formed on the surface of helium droplets. The ν_1 CH stretch ro-vibrational spectra were measured revealing what appears to be the *P* and *R* contours of a nearly rigid linear rotor. To simulate the linear molecule spectra, given a rotational temperature of 0.37 K, effective moments of inertia, I_B, were required to be 10^4-10^5 amu·Å^2 larger than the ab initio predicted values. The large moments of inertia were found to be strongly dependent on both the mass of the complex and the size of the helium droplet, consistent with a model where the dopant is located in a dimple site on the surface of the droplet. In this model, the moment of inertia is representative of the rotational motion of the dopant on the surface about an inertial axis through the center of the droplet.

1. Introduction

The electronic spectra of alkali atoms implanted in bulk superfluid helium were reported in the early 1990s.[1−3] These studies were motivated in part by the long-standing interest in the interactions of foreign impurities with superfluid helium and also by the prospect of isolating alkali atom clusters in a weakly interacting, cold matrix. Clusters of alkali atoms are of fundamental importance, serving as prototypical models of finite quantum systems. Unfortunately, the violent laser sputtering method employed for implantation lead to rather poor control over the species produced in the liquid. Consequently, no covalently bound molecules or van der Waals complexes were observed in these studies. At about the same time, much of the focus on liquid helium droplets was centered on their potential to serve as gentle matrices for the spectroscopic interrogation of dopant species,[4−6] including clusters of alkali atoms. Substantially better control over the production of alkali clusters was achieved in the pioneering work of Scoles et al.,[7] which involved the sequential pick-up of alkali atoms by large ($N \approx 10^4$) liquid helium droplets. The size and composition of the alkali cluster picked up by the helium droplets were controlled by simply changing the pressure of the alkali vapor in one or more "pick-up" cells.[8−11] Alkali atoms and clusters proved to be ideal systems to use as probes of dopant droplet interactions, given their theoretical tractability, known absorption spectra, and weak perturbations of the helium solvent.

The laser induced fluorescence (LIF) excitation and dispersed emission spectra of Li,[12] Na,[10−14] K,[12,13] Rb,[15,16] and Cs[17] atoms attached to helium droplets have been reported for the $n^2P_{3/2}$, $n^2P_{1/2} \leftarrow n^2S_{1/2}$ transitions (D_1 and D_2 lines). In comparison to the large blue shifts and broad line widths observed upon excitation in the bulk,[2] small ($\sim$10 cm^{-1}) solvent shifts and narrower line widths were observed in the droplet studies. The observed shifts and line widths provided strong evidence that the alkali atoms were attached to the surface of helium droplets upon pick up. Additionally, the LIF excitation spectra all had characteristic tails to the blue, assigned as transitions from bound to continuum states, with the atom desorbing from the droplet.[12] Subsequent theoretical calculations[18,19] and experiments confirmed that, indeed, the alkali atoms were located in a dimple on the surface of the droplets. The experiments included the observation of M*He exciplex formation[13,15−17,20,21] and the determination that penning ionization is the operative charge-transfer mechanism in alkali, helium droplet mass spectrometry at low electron impact energies (<24 eV).[22,23]

It was also shown that the pick-up of multiple alkali atoms favored the formation of high spin species,[7,11,24−27] providing compelling examples of the cluster formation process occurring on the surface of helium droplets, which allows for the formation of species that would be difficult, if not impossible, using standard gas-phase molecular beam techniques. Complexation of two alkali atoms with their spins antiparallel results in a covalent bond, and the collisional cooling in a gas-phase expansion favors the formation of this lower energy singlet dimer. However, in helium droplets, the triplet Na_2 complex is favored over the singlet species by a ratio of 10 000:1.[24] Formation of the dimer on the singlet potential results in its evaporation from the surface of the droplet, as a consequence of the larger binding energy of the singlet dimer (6000 cm^{-1}) in comparison to that of the triplet dimer (170 cm^{-1}).[28] Quartet spin states of the alkali trimers have also been reported,[28−30] and spin polarized potassium clusters with as many as 25 atoms have been shown to be stable on the surface of helium droplets.[31]

It is not surprising that alkali atoms and clusters reside in dimple sites on the surface of helium droplets, given that the M−He interatomic interactions are some of the weakest interactions found in nature.[32,33] The weakly attractive interaction of an alkali atom and a helium atom originates from the Pauli repulsion of the *s* valence electrons. In fact, the Na−He interaction is at longer range and less attractive than the He−He interaction. As a result, alkali atoms in helium droplets have

† Part of the "Roger E. Miller Memorial Issue".

* Corresponding author: douberly@uga.edu.

‡ Current address: Department of Chemistry, The University of Georgia, Athens, GA 30602.

§ Deceased: November 6, 2005.

10.1021/jp070042a CCC: $37.00
Published on Web 06/29/2007

a positive energy of occlusion[34] and are expelled to the surface upon pick up. To predict if a dopant becomes solvated upon pick up by a helium droplet, Ancilotto and co-workers have defined a simple empirical dimensionless parameter based upon helium density functional calculations using model Lennard-Jones potentials.[35] The Ancilotto parameter,

$$\lambda \equiv \frac{\rho \epsilon r_{\min}}{\sigma 2^{1/6}} \quad (1)$$

($\sigma = 0.179$ cm^{-1} Å^{-2} is the surface tension of liquid helium, $\rho = 0.0218$ Å^{-3} is the density of liquid helium, and ϵ and $r_{\min}$ are the equilibrium well depth and bond distance, respectively) is simply a measure of the ratio of the dopant−helium attraction to the energy cost of forming a helium surface upon solute solvation. While the energy cost of forming a cavity of radius R is proportional to σR^2, the energy gain scales as $\epsilon \rho R^3$ because of the attractive dopant−helium pair potential. Ancilotto et al. predicted that dopants with $\lambda \approx 1.9$ would be solvated, which should be compared with the values for the alkali metals, namely, $\lambda \approx 0.7$. Certainly, the Ancilotto model correctly predicts the surface bound location of the alkali atoms. In comparison, molecular dopants such as HCN or SF_6 have large (>20) Ancilotto parameters[35] and are indeed solvated within the droplet.[36,37]

It has been demonstrated[38] that a dopant bound to the surface may become solvated if a solvated species is also present in the droplet. For example, Vilesov and co-workers found that the chemiluminescent Ba + $N_2O \rightarrow$ BaO* + N_2 reaction was enhanced if xenon atoms were first added to the helium droplets. As a result of the long-range attractive interaction of the solvated Xe_{15} cluster and the surface bound Ba atom ($\lambda \approx 1.7$),[39] the Ba atom was effectively "sunk", suppressing the reaction channel corresponding to the hot products desorbing from the droplet and radiating in the gas phase. In the current report, we address the question of whether a polar dopant such as HCN can form complexes with the surface bound alkali metals. Trapping alkali−adsorbate systems in helium droplets would provide an ultra-cold environment for the study of harpooning[40−45] and charge transfer[46,47] reactions, including the stabilization of reaction intermediates. We use an infrared laser to excite the CH stretch of the HCN chromophore near 3 μm and look for spectral signatures which provide clues regarding the location of the dopant relative to the center of the droplet and the associated solvent−solute interactions. The CH stretch vibrational bands of the HCN−M species display what appears to be the P and R contours of the spectrum of a linear rotor with an effective moment of inertia approximately 200 times larger than the value predicted from high level ab initio calculations. Additionally, the degree to which the moment of inertia is enhanced is strongly correlated with the size of the droplet to which the HCN−M species is isolated.

2. Experimental Method

The helium droplet apparatus used in the present study has been recently reviewed in detail.[48] The helium droplets are formed by expanding ultrahigh purity helium into vacuum through a 5 μm diameter nozzle operated typically at 60 bar and 20 K. Droplet formation is a statistical process, and the mean droplet size can be controlled by simply changing the nozzle temperature from 14 to 30 K, producing sizes in the range 1000 to 20 000 helium atoms. We emphasize that the mean droplet sizes reported here for various nozzle conditions are estimates determined from published scaling laws.[49] The nozzle temperature is controlled with a PID feedback loop consisting of a Kaptan heater, Lakeshore Si diode sensor, and a Lakeshore model 321 temperature controller, which results in a temperature accuracy of ±0.05 K. The droplet expansion is collimated by a 0.4 mm conical skimmer. We have previously demonstrated that metal−cluster adsorbate systems (HCN−Mg_n) are readily formed in helium droplets by the separate pick up of Mg atoms and an HCN molecule.[50−52] The Mg atoms ($\lambda \approx 2.6$)[39] are picked up and solvated[53] by the helium droplets by passing the droplet beam through a resistively heated oven. Downstream, the droplets pass through a 4 cm long gas pick-up cell containing HCN, which in turn leads to the condensation of the HCN−Mg_n complex within the droplet. The temperature of the oven is varied, and the droplets pick up an average number of atoms determined by the vapor pressure of the metal at the oven temperature.[48] An identical approach is used to dope the droplets with alkali atoms. The vapor pressure required to dope the droplets on average with one alkali atom is approximately 10^{-4} Torr, corresponding to sample temperatures of 215, 160, 100, and 60 °C, for Na, K, Rb, and Cs, respectively.[54] Since the required temperature is higher than the melting temperature of the metal (98, 64, 39, 28 °C/Na, K, Rb, Cs), the oven was introduced through a load lock located at the top of the pick-up chamber of the apparatus. The metal is located in the bottom of the oven, and the droplet beam passes through a scattering cell filled with the metal atom vapor above the melted sample. The scattering cell is closer than the sample to the heat source (cartridge heater) to prevent metal condensation on the cell walls. The pressure of HCN in the gas pick-up cell is maintained at 2×10^{-6} Torr, namely, the pressure required to dope each droplet with one HCN on average.

Downstream from the pick-up zone, vibrational excitation of the HCN−M complexes is carried out with an F-Center laser (Burleigh FCL-20), operating on crystal No. 3 (RbCl:Li), pumped by 1.5 W of red light from a krypton ion laser (Coherent Sabre). Details of the tuning and calibration of this laser are given elsewhere.[55] The laser interaction region consists of two parallel gold mirrors such that multiple passes of the infrared laser intersect the droplet beam. Additionally, the laser interaction region is equipped with Stark electrodes such that a dc electric field can be applied orthogonal to both the path of the droplet beam and the laser. The linearly polarized laser is oriented such that the laser electric field vector is parallel to the static dc Stark field. A liquid helium cooled bolometer detector monitors the on axis droplet beam flux. An infrared spectrum is acquired by monitoring the laser induced beam depletion that results from the evaporation of helium atoms following the transfer of the HCN−M excited vibrational energy to the droplet.

3. Theoretical Methods and Results

Using Molpro,[56] ab initio calculations at the RMP2 and RCCSD(T) levels were carried out for the lowest energy, nitrogen bound HCN−M complexes to determine the rotational constants, dipole moments, and vibrational frequency shifts from the HCN monomer. The ab initio results are summarized in Table 1. For both of the ab initio methods, all electrons were correlated. Throughout, an aug-cc-pVTZ basis set was used for HCN, while a 6-311++G(2d,2p) basis set was used for Li, Na, and K. Effective core potentials (ECP, Stuttgart RSC ECP 1997) from the Gaussian basis set library were used for Rb and Cs.[57,58] The ECP basis sets for Rb and Cs consist of 9 valence electrons, with the remaining electrons being in the core.

The counterpoise corrected[59] RCCSD(T) intermolecular potential surface for HCN−Na is shown in Figure 1, showing

TABLE 1: Summary of the Ab Initio and Experimental Constants for the HCN−M Complexes

HCN−M	Li	Na	K	Rb	Cs
	ab initio (RMP2)				
B'' (cm^{-1})	0.337	0.124	0.0810	0.0576	0.0500
μ_{RHF} (Debye)	8.62	7.58	7.86	7.62	7.65
μ_{UMP2} (Debye)	7.92	6.81	6.48	6.61	6.44
D_e (cm^{-1})	2350	842	1025	819	775
r_{N-M} Å	2.048	2.561	2.909	3.101	3.209
$\Delta\nu$ (cm^{-1})	−12.4	−9.2	−8.7	−8.9	−7.6
	ab initio (RCCSD(T))				
B'' (cm^{-1})	0.340	0.126	0.0809	0.0584	
μ_{RHF} (Debye)	8.63	7.60	7.85	7.64	
D_e (cm^{-1})	2460	877	1026	805	
r_{N-M} Å	2.038	2.548	2.917	3.079	
	experimental				
μ'' (Debye)		6.9(1)	6.6(1)	6.6(1)	6.7(1)
μ' (Debye)		7.0(1)	6.7(1)	6.7(1)	6.8(1)
$\Delta\nu$ (cm^{-1})		−8.01	−8.40	−8.24	−8.04
T_{rot} (K)		0.37	0.37	0.37	0.37
B'' (MHz) ($\bar{N} = 7200$)					
0 V/cm		15.6	9.3	6.8	4.9
510 V/cm		4.2	3.6	2.0	1.3
I amu-Å^2 ($\times 10^4$) (0 V/cm)		3.24	5.42	7.43	10.3
I amu-Å^2 ($\times 10^5$) (510 V/cm)		1.12	1.40	2.50	3.75
$B_{ab\ initio}/B_{0V/cm}$		239	261	251	306
$B_{ab\ initio}/B_{510V/cm}$		889	675	854	1152

the linear nitrogen bound HCN−Na complex as the global minimum with a binding energy of 877 cm^{-1}. In comparison, the restricted Hartree−Fock (RHF) binding energy is 633 cm^{-1}, indicating that most of the interaction energy is electrostatic and can be attributed to the dipole-induced polarization of the Na atom. Given the strong interaction, if the two subunits can approach one another within the droplet, then it seems likely that they will form the complex. However, complex formation may occur near the surface of the droplet, and it is not clear whether or not the condensation energy released will desorb the complex from the surface.

Assuming the complex forms and remains bound to the droplet, it is interesting to consider the He−dopant intermolecular interaction, which will largely determine the sign of the occlusion energy. Figure 2 shows a comparison between the RMP2 He−HCN and He−HCN−Na potentials. While the He−HCN potential is attractive on each end of the molecule, the He−HCN−Na potential is quite repulsive on the sodium end of the complex. The He−Na pair potential at the same level of theory has an equilibrium well depth and bond distance of −0.586 cm^{-1} and 6.95 Å, respectively. Comparing these values to the one-dimensional (1D) slice of the He−HCN−Na potential ($y = 0$) indicates that the helium is less attracted to the sodium end of the complex than it is to the bare Na atom. At the same time, the helium is more attracted to the hydrogen end of the complex than to the bare HCN molecule. This is consistent with the dipole induced polarization of the Na atom, which results in a buildup of electron density on the Na end of the complex, while electron density is removed from the area near the hydrogen atom. This type of heliophilic, heliophobic interaction is reminiscent of the types of interactions between amphiphilic molecular species and liquid water. Given the He−dopant potential, the Na end of the complex will prefer to be on the surface while the hydrogen end will prefer to be solvated. Whether or not the balance of the two forces results in a "sunk" complex is still unclear. However, it is clear that a condensed HCN−Na species will be strongly bound to the droplet, and if indeed the complex becomes solvated, there will be excluded helium from the region around the Na atom.

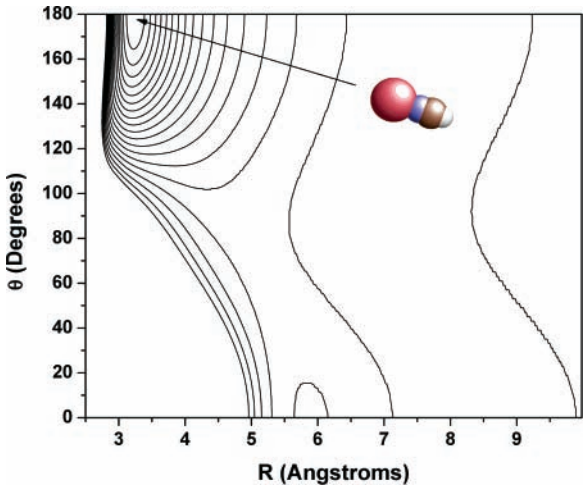

Figure 1. Counterpoise corrected intermolecular potential energy surface for the HCN−Na complex obtained at the RCCSD(T) level of theory. The d-aug-cc-pVTZ basis set was used for HCN, and the cc-pVTZ basis set was used for Na. The Jacobi coordinate, R corresponds to the distance from the Na atom to the center of mass of HCN, while θ correspond to the Na, HCN center of mass, H atom angle. The intramolecular HCN degrees of freedom were optimized at each point on the potential energy surface. The global minimum corresponds to the linear HCN−Na geometry with a binding energy equal to −877 cm^{-1}. Contours range from −850 to 100 and are separated by 50 cm^{-1}.

4. Experimental Results

4.1. HCN−Na Complex: Extreme Moment of Inertia Enhancement. The pendular state spectra[60,61] in Figure 3 were recorded by applying a large static dc electric field to the laser interaction region and tuning the infrared laser through the free CH stretching region of HCN in helium droplets. With the Na oven at room temperature, the top spectrum was recorded, corresponding to the pendular spectrum of the $(HCN)_n$ linear chains,[62] with the HCN monomer band at 3311.20 cm^{-1}. The HCN monomer signal intensity was maximized by adjusting the pressure of the HCN gas in the gas pick-up cell. To estimate the optimal conditions for the production of HCN−Na, the Na oven temperature was increased until the HCN signal was decreased by approximately 40%, assuming the loss of signal originates from intensity being shifted to the complex. The bottom pendular spectrum was recorded with the sodium oven at 200 °C, and a new band at 3303.19 cm^{-1} appeared. The assignment of the new band to the ν_1 fundamental transition of HCN−Na is supported by several observations: (i) the pressure (2×10^{-6} Torr) in the pick-up cell required to optimize the signal intensity is indicative of a species that contains only one HCN molecule; (ii) the signal depends strongly on oven temperature and is maximized at 215 °C, which approximately corresponds to the temperature required to produce a 10^{-4} Torr sodium vapor pressure;[54] and (iii) the frequency shift (−8.01 cm^{-1}) agrees well with the ab initio frequency shift reported in Table 1.

The pendular spectra for the other HCN−M (M = K, Rb, Cs) complexes (discussed below) were obtained and assigned in the same way as described here. However, it is interesting to note that, for all of the spectra, the signal intensity of the HCN−M pendular band was optimized at nozzle conditions corresponding to the larger droplet sizes, namely, $N > 10\,000$. In addition, the signals became larger as the complex became heavier, HCN−Cs having the largest signal. While the ab initio calculations do not show enough variation in the oscillator strengths to account for the observed differences, it has been determined that the heavier alkali atoms bind more strongly to

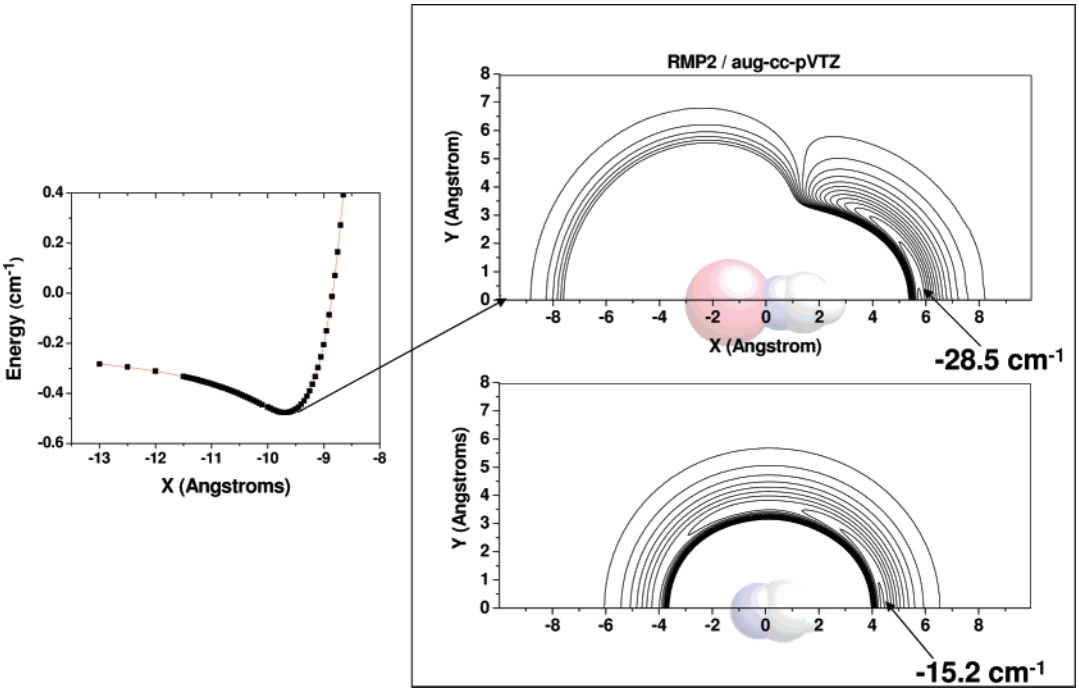

Figure 2. Comparison of the He dopant potentials for the HCN monomer and the HCN−Na binary complex. The counterpoise corrected potential energy surfaces were obtained at the RMP2 level of theory with an aug-cc-pVTZ basis set for all atoms. The contours range from −28 to 0 with 2 cm^{-1} intervals. The origins correspond to the centers of mass of the molecule or the complex. The 1D plot corresponds to the $Y = 0$ slice of the He−HCN−Na potential surface, having an equilibrium bond distance and well depth of −9.67 Å and −0.477 cm^{-1}, respectively.

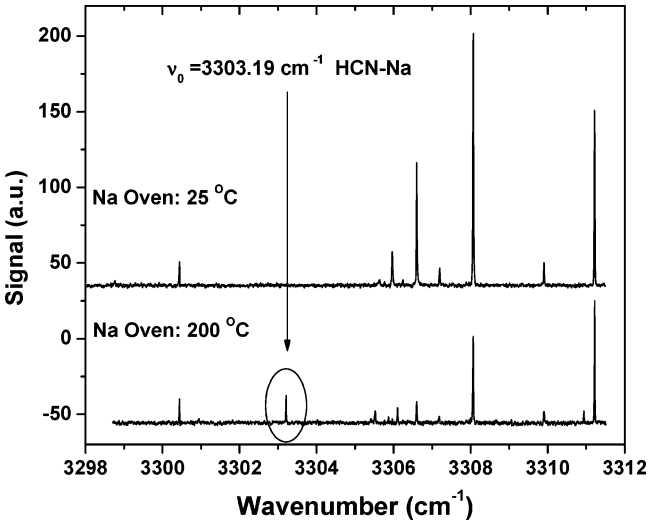

Figure 3. Pendular state spectra of the HCN free CH stretching region with the sodium oven cold (top) and the sodium oven at approximately 200 °C (bottom). The source conditions produced a mean droplet size of approximately 7200 helium atoms. The applied electric field strength was ∼30 kV/cm.

the droplet surface.[19,63] In fact, the binding energy of an alkali atom to the droplet is predicted to increase with droplet size, varying according to $S(N) = S_0 + S_1/N^{1/3} + S_2/N^{2/3}$, with the binding energy of a Na atom in the large droplet limit being $S_0 = -12.1$ K.[19] Given the weak binding of the atom to the cluster surface, it is likely that a fraction of the adsorbed alkali atoms are ejected from the surface of the droplet upon pick-up of the HCN molecule in the downstream, gas pick-up cell. The fraction of atoms ejected would then vary with droplet size and mass of the atom, accounting, in part, for the variation in signal intensities observed in the present work. Additionally, for the larger droplets, the initial increase in droplet temperature is less upon HCN pick-up, which in turn reduces the rate of desorbtion of the alkali atom in comparison with the smaller droplets. It is also interesting to note, that despite many attempts, the HCN−Li complex could not be produced, even if the order of pick-up was reversed, picking up the lithium atom second. The failure to produce the HCN−Li complex is likely partially due to the weak binding and high zero-point energy of Li attached to the droplet.

The droplet size dependence of the ν_1 fundamental pendular band of HCN−Na is shown in Figure 4, with the mean droplet size varied from $\bar{N} = 7200$ to $\bar{N} = 2050$ (top to bottom of the figure). The nozzle temperature was varied from 18 to 24 K. It is clear that the HCN−Na signal intensity decreases for the smaller droplet sizes. For comparison, the HCN $Q(0)$ line is shown for a wider range of droplet sizes, with signal persisting to much smaller average sizes. Besides the differing droplet size conditions that optimize the signal, the two sets of spectra are rather similar, both pendular bands broadening and shifting to the blue as the average droplet size is reduced, an effect which has been discussed in detail elsewhere.[64]

Turning off the pendular field and reducing the nozzle temperature to 16.5 K to produce larger droplets, we recorded the zero-field spectrum of HCN−Na which is shown in Figure 5. Here, we initially assumed that the unresolved substructure of the zero-field band corresponded to the P and R contours of a linear rotor spectrum. It is important to point out, since individual HCN−Na ro-vibrational transitions are not resolved, it is impossible to uniquely determine both the B constant and the rotational temperature, T_{rot}, by fitting the P and R contours using a linear rotor Hamiltonian. Nevertheless, the product of B and kT_{rot} can be determined and, hence, B if we assume that $T_{rot} = 0.37$ K, namely, the rotational temperature typical of solutes that have vibrational spectra displaying resolved rotational fine structure.[6] In Figure 5, the smooth line is a simulated rigid linear rotor spectrum, using a rotational constant of $B'' = 9.4$ MHz, assuming a rotational temperature of 0.37 K. While a P and R branch linear rotor spectrum was anticipated, it was

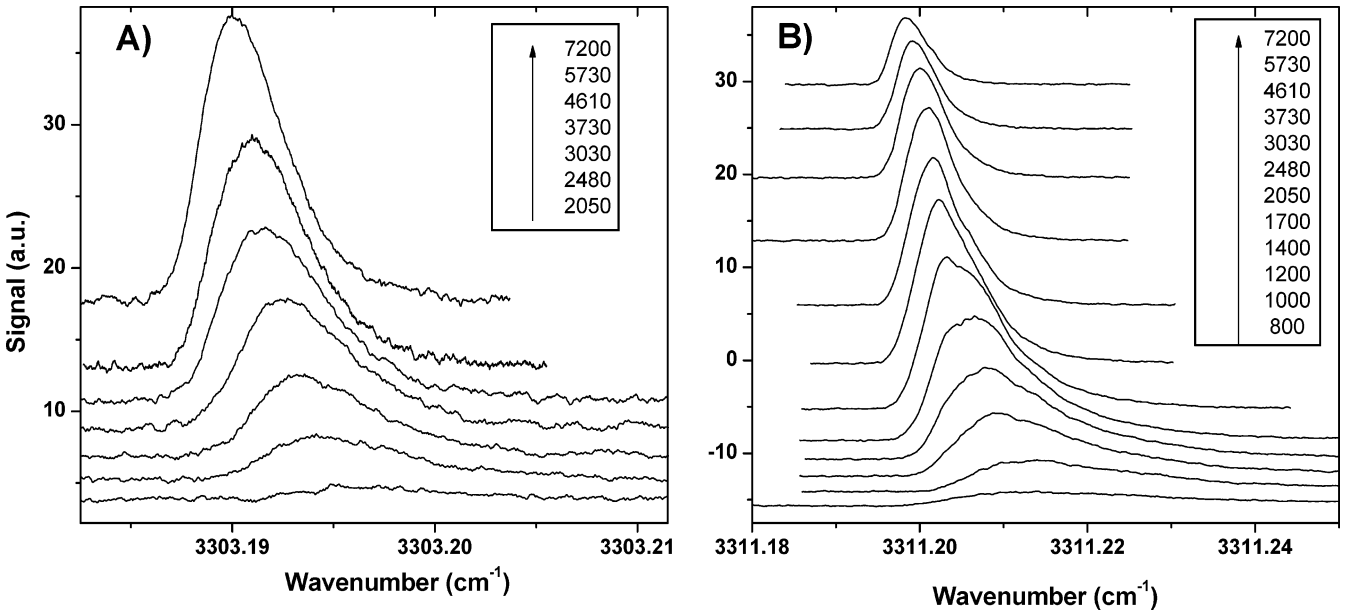

Figure 4. (A) Droplet size dependence of the HCN−Na pendular spectrum. The largest droplet size used was on average 7200 helium atoms. The mean size increases from bottom to top. (B) Also shown for comparison is the analogous droplet size dependence of the $Q(0)$ line of the HCN monomer.

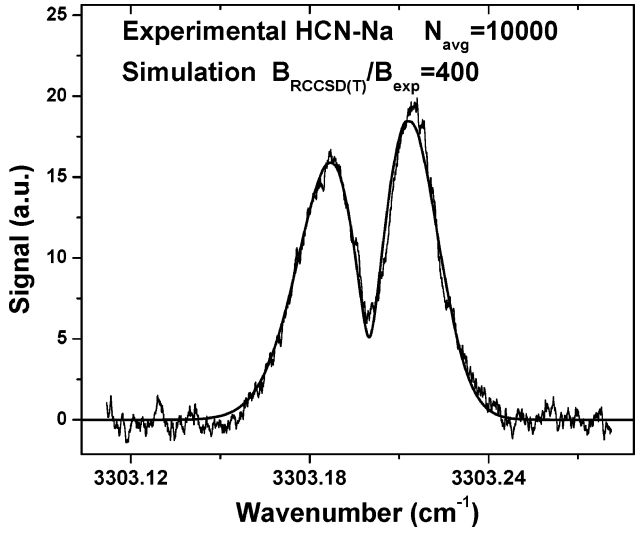

Figure 5. Zero-field spectrum of the HCN−Na complex, along with a linear rotor simulation with constants $B'' = 9.4$ MHz, $T_{rot} = 0.37$ K, and a Lorentzian line shape with a fwhm of 100 MHz. The source conditions (60 bar, 16.5 K) resulted in helium droplets with a mean size of approximately 10 000 helium atoms.

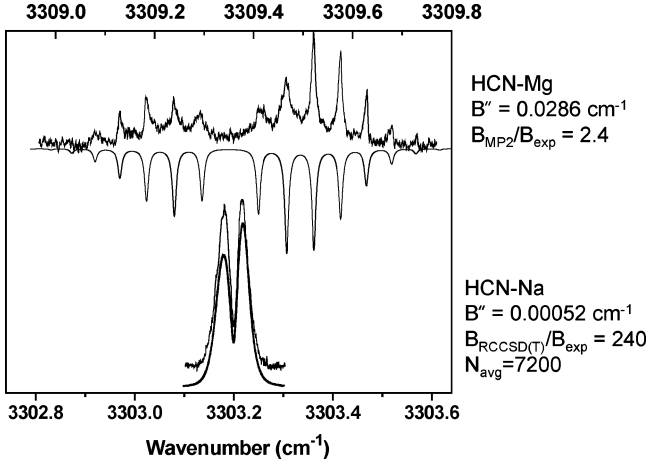

Figure 6. Comparison of the HCN−Mg and HCN−Na zero-field spectra. $T_{rot} = 0.37$ K for both simulations, and a 250 MHz fwhm Lorentzian line shape was used for the HCN−Mg simulation, while a 100 MHz fwhm line shape was used for HCN−Na. Each spectrum was obtained at 60 bar and 18.0 K source conditions, corresponding to a mean droplet size of 7200 helium atoms.

quite surprising to find that the moment of inertia of the rotational motion was 5.3×10^4 amu·Å^2. In Figure 6, the HCN−Na spectrum is compared with the HCN−Mg spectrum,[50] both spectra recorded under similar droplet source conditions ($\bar{N} =$ 7200). Fitting the HCN−Mg spectrum to a linear rotor Hamiltonian gives a rotational temperature of 0.37 K and a B'' rotational constant 2.4 times smaller than the ab initio constant. A factor of 2.4 reduction in the rotational constant is consistent with what has come to be expected for helium solvated rotors with anisotropic He−dopant potentials,[65−67] the added moment of inertia originating from a normal fluid component of the liquid He rotating rigidly with the complex. If the profile of the zero-field spectrum is indeed the P and R contours of a linear rotor with $T_{rot} = 0.37$ K, then the HCN−Na rotational constant is reduced by a factor of 240 ($B'' = 15.6$ MHz). Apparently, the solvent−solute interactions discussed above significantly alter the rotational dynamics of the HCN−Na complex in comparison with altering that of HCN−Mg.

Comparing the HCN−Na zero-field spectra shown in Figures 5 and 6, we find the rotational constant has apparently increased upon changing the average droplet size from 10 000 to 7200 helium atoms. While the shapes of rotational lines have been observed to be droplet size dependent, as a result of inhomogeneous broadening, there is no other example, to our knowledge, of a rotational constant that varies so dramatically with droplet size. Certainly, the rotational constant of HCN−Mg was constant over a wide range of sizes, within the experimental error.

If we assume that T_{rot} is constant, then we can measure the variation of B'' with average droplet size by simply changing the nozzle temperature. Figure 7 shows the zero-field spectrum of HCN−Na recorded for a range of source conditions (16.5−22.0 K). If the HCN−Na band profiles are indeed the P and R contours of unresolved substructure of a linear molecule

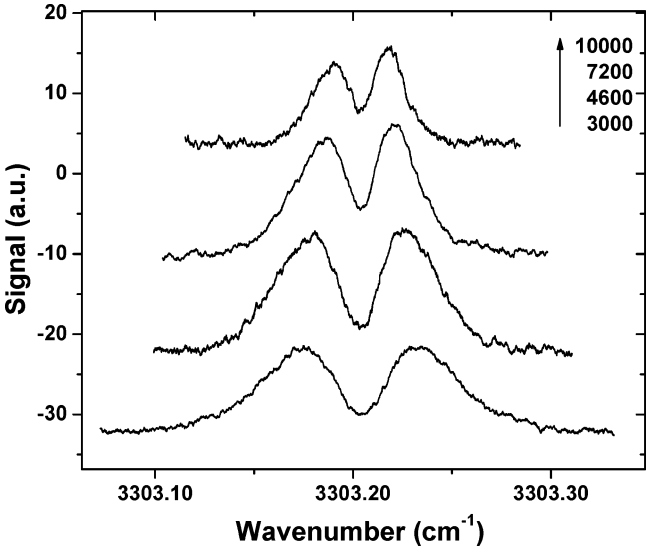

Figure 7. Droplet size dependence of the HCN−Na zero-field spectrum. The mean droplet size increases from bottom to top and ranges from ∼3000 to ∼10 000 helium atoms.

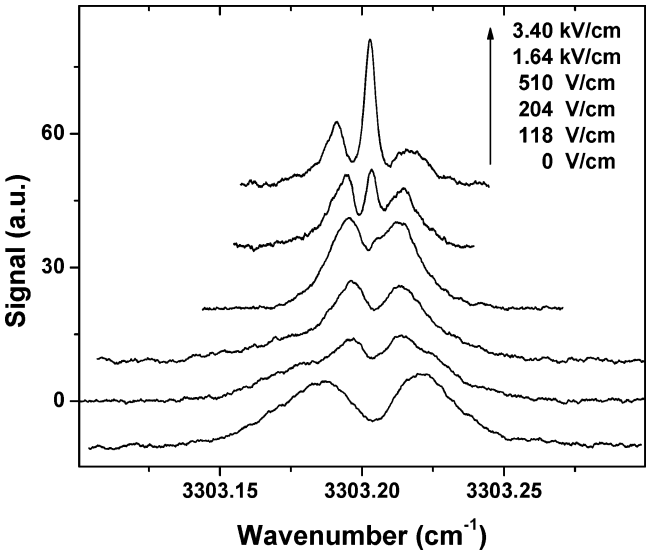

Figure 8. Evolution of the spectrum of the CH stretch of the HCN−Na complex with increasing Stark field strength. The nozzle conditions were fixed at 60 bar and 18.0 K ($\bar{N} = 7200$), and the Stark field was increased as shown in the legend (increasing field from bottom to top).

spectrum, then a reduction in the average droplet size from 10 000 to 3000 results in an increase in B'' by a factor of 5 (I_B decreases by 4.3×10^4 amu·Å^2), clearly not a minor effect.

4.2. Stark Spectra of the HCN−Na Complex. The evidence discussed above provides considerable support to the assignment of the pendular band at 3303.19 cm^{-1} to the HCN−Na complex. To provide further support to the assignment, we also measured the Stark spectra of the 3303.19 cm^{-1} band at intermediate field strengths with the intention of determining the dipole moment of the complex. The series of spectra shown in Figure 8 were recorded at various Stark field strengths, as shown in the legend, with the field strength increasing from bottom to top. The average droplet size was held constant throughout the series of spectra.

Once again, we assume $T_{rot} = 0.37$ K throughout, and we obtain rotational constants by fitting the apparent P and R contours of the spectra. Upon fitting the Stark spectrum at low field, we found that an additional enhancement of the moment of inertia was required to obtain satisfactory agreement between the simulation and the experiment. The rotational constant of the spectrum recorded at 510 V/cm corresponds to $B'' = 4.2$ MHz, compared with $B'' = 15.6$ MHz for the zero-field spectrum. The rotational constant, reduced by a factor of 3.7 from the zero-field value, does not appear to change further with increasing field strength. In addition, there does not appear to be a smooth transition in the rotational constant, going from zero-field to 510 V/cm. Instead, the spectrum recorded at 118 V/cm appears to be a superposition of two spectra, each having a different B'' constant. The zero-field spectrum appears as a broad background in the 204 V/cm spectrum and disappears entirely once the field has reached 510 V/cm. Suprisingly, application of a modest Stark field apparently provides a mechanism to increase the moment of inertia by 7.96×10^4 amu·Å^2, again, not a minor effect. Table 2 provides a summary of ΔI_B between the 510 V/cm and the 0 V/cm HCN−M spectra recorded with the mean droplet size set to ∼7200 helium atoms. In addition, a small, approximately 50 MHz, blue shift is observed upon application of the 118 V/cm field. With increasing field, the spectrum appears to shift back to the red, which is typical of the Stark spectrum of a linear molecule that has an increase in the permanent dipole moment in the excited vibrational state.

TABLE 2: Summary of the Best Fit Parameters for the HCN−M Droplet Size Dependent Rotational Constant Analysis[a]

HCN−M	Na	K	Rb	Cs
	zero-field (eq 2)			
M (amu)	50	66	112	160
a (amu)	−29(3)	−38(4)	−72(3)	−104(5)
b ($\times 10^3$ He atoms)	1.8(3)	1.1(2)	0.4(2)	0.3(4)
	zero-field (eq 3)			
M (amu)	50	66	112	160
a (amu)	25	25	25	25
b ($\times 10^3$ He atoms)	1.8(3)	1.1(2)	0.4(2)	0.3(4)
α	3.7(6)	3.2(4)	3.4(3)	3.3(3)
	510 V/cm (eq 2)			
M (amu)	50	66	112	160
a (amu)	15(3)	24(3)		
b ($\times 10^3$ He atoms)	0.4(1)	0.71(9)		
	510 V/cm (eq 3)			
M (amu)	50	66	112	160
a (amu)	25	25		
b ($\times 10^3$ He atoms)	0.4(1)	0.71(9)		
α	1.16(5)	1.02(3)		
ΔI (510 V/cm − 0 V/cm) ($\times 10^4$ amu-Å^2)	7.93	8.57	17.6	27.2

[a] ΔI (510 V/cm − 0 V/cm) corresponds to the enhancement of the moment of inertia upon application of the 510 V/cm Stark field with $\bar{N} = 7200$, assuming $T_{rot} = 0.37$ K.

A simulation of a linear molecule Stark spectrum, fixing the B'' constant to the value obtained at 510 V/cm, provides an estimate of the HCN−Na dipole moment. The simulation of the Stark spectrum recorded at 6.75 kV/cm, shown in Figure 9 (smooth line), was produced with ground and upper vibrational state dipole moments of 6.9 and 7.0 Debye, respectively. Although the experimental error bars are large (±0.2 Debye), the UMP2 dipole moment, $\mu_{UMP2} = 6.81$ Debye, is in good agreement with the experimental values, providing further support to the HCN−Na assignment.

4.3. HCN−M (M = K, Rb, Cs). The analogous spectra were obtained for the HCN−M (M = K, Rb, Cs) complexes, applying the same technique described above. The ν_1 fundamental bands of the binary HCN−M complexes are all located within 1 cm^{-1}

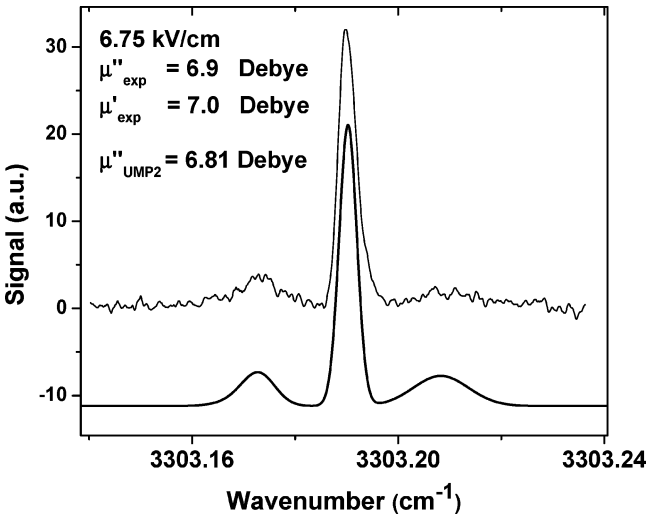

Figure 9. Stark spectrum of HCN−Na obtained with a 6.75 kV/cm field strength. The nozzle temperature was 18.0 K, producing a mean droplet size equal to 7200 helium atoms.

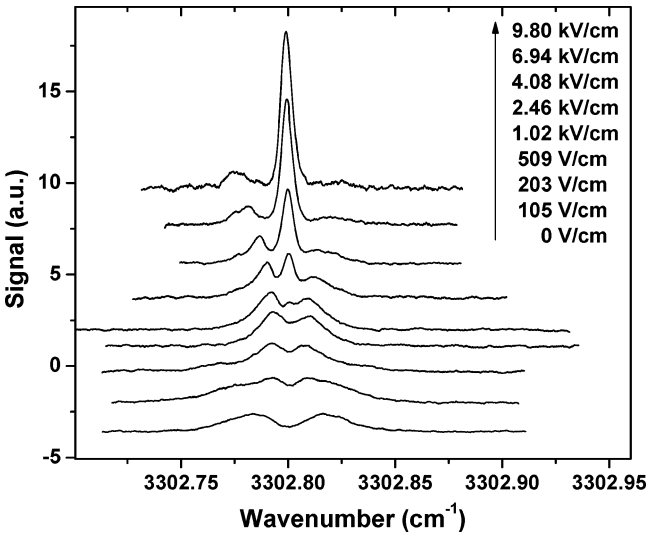

Figure 10. Evolution of the spectrum of the CH stretch (3302.80 cm^{-1}) of the HCN−K complex with increasing Stark field strength. The nozzle conditions were fixed at 60 bar and 19.0 K ($\bar{N} = 6000$), and the Stark field was increased as shown in the legend (increasing field from bottom to top).

from the HCN−Na band origin. In the HCN−K pendular spectrum, a band centered at 3302.80 cm^{-1} is assigned to the binary HCN−K complex, and the evolution of the band with increasing Stark field strength (Figure 10) is similar to the HCN−Na spectrum. Once again, a large effective moment of inertia is required to simulate the zero-field spectrum, assuming a linear rotor Hamiltonian. I_B increases further with the application of the Stark field. In addition, the band origin of the ∼510 V/cm Stark spectrum is shifted by approximately 50 MHz to the blue, relative to the zero-field spectrum. The only difference between the HCN−Na and the HCN−K spectra is a slight increase in the effective moment of inertia at the same average droplet size, which is reasonable, given the HCN−K complex is 16 amu heavier. The rotational constants for the HCN−M complexes at $\bar{N} = 7200$ are compared in Table 1.

The zero-field and Stark spectra of the HCN−Rb and HCN−Cs bands centered at 3302.96 cm^{-1} and 3303.16 cm^{-1} are shown in Figures 11 and 12, respectively. Once again, all of the features observed for the HCN−Na and HCN−K spectra are reproduced. The bottom spectrum in each figure corresponds to zero-field

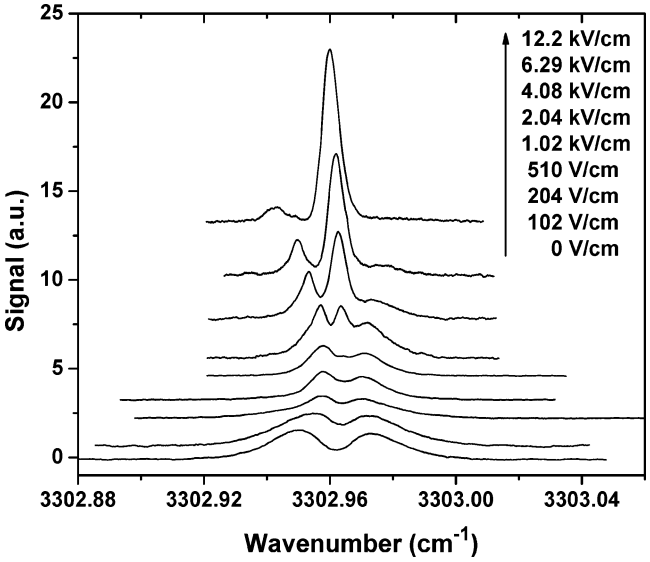

Figure 11. Evolution of the spectrum of the CH stretch of the HCN−Rb complex (3302.96 cm^{-1}) with increasing Stark field strength. The nozzle conditions were fixed at 60 bar and 18.0 K ($\bar{N} = 7200$), and the Stark field was increased as shown in the legend (increasing field from bottom to top).

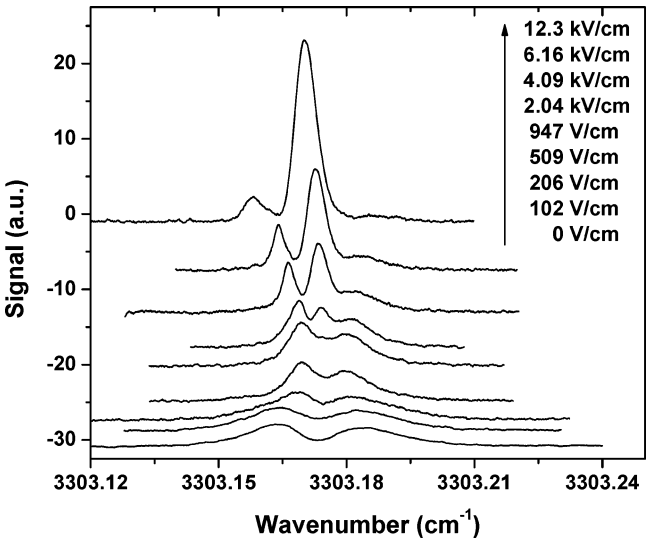

Figure 12. Evolution of the spectrum of the CH stretch of the HCN−Cs complex (pendular band at 3303.16 cm^{-1}) with increasing Stark field strength. The nozzle conditions were fixed at 60 bar and 18.0 K ($\bar{N} = 7200$), and the Stark field was increased as shown in the legend (increasing field from bottom to top).

conditions and is again characteristic of a rotor with a large effective moment of inertia. Again, as the Stark field strength increases, the moment of inertia increases, and a small blue shift of the CH stretch vibrational band orgin is observed, consistent with the other HCN−M spectra. The dipole moments obtained from simulations of all HCN−M Stark spectra are summarized in Table 1, all in good agreement with the ab initio UMP2 results.

5. Discussion

Formation of the HCN−M complex is likely occurring on or near the surface of the helium droplet. With the alkali atom residing in a surface dimple, the droplet collides with an HCN molecule. Although the HCN molecule could initially become solvated, the HCN−droplet potential is flat near the droplet center,[68] such that it can approach the surface. The long-range

attractive HCN−M potential could then steer the HCN molecule toward the alkali atom, resulting in complex formation. However, the final location of the dopant relative to the surface of the droplet will depend on the sign of the occlusion energy. If the free energy gain upon solvation is greater than the free energy cost of helium cavitation, then the complex will sink. If solvation leads to an increase in the systems free energy, then it will remain on the surface. The He−HCN−Na interaction potential suggests that an HCN−Na complex placed at the center of a droplet would create a cavity with an ∼12 Å diameter centered at $\sim x = -4$ Å (see Figure 2). A surface bound location seems likely, especially considering that the free energy could be reduced by orienting the complex toward the center of the droplet such that the hydrogen end becomes solvated, while the sodium end of the complex resides on the surface.

A comparison of the experimental and ab initio dipole moments and frequency shifts provides strong support to the assignments of the HCN−M (M = Na, K, Rb, and Cs) spectra. In addition, the assignments are supported further when each band's dependence on the HCN pick-up cell pressure and alkali oven temperature is considered. We emphasize again that the zero-field band shapes are interpreted as the *P* and *R* contours of a linear rotor spectrum, lacking resolved rotational fine structure. We have also assumed $T_{rot} = 0.37$ K, a value obtained from molecular dopants whose ro-vibrational spectra display rotational fine structure. With these assumptions, the HCN−M rotational constants are anomalously small, corresponding to rotors having extremely large effective moments of inertia, especially in comparison with the ab initio HCN−M values (Table 2). Additionally, the moments of inertia are strongly correlated with the average droplet size. Given the support for the assignments discussed above, it is likely that both the enhanced moments of inertia and their size dependence are reflective of the unique HCN−M rotational dynamics, previously unobserved for molecular rotors solvated in helium droplets.

To account for the anomalously large moments of inertia, we initially considered two models. Since $I = MR^2$ in the rigid rotor approximation, either the dopant has become effectively more massive, as a result of helium following the dopant rotational motion, or the axis of rotation has been shifted from the center of mass of the HCN−M complex. For example, consider the zero-field spectrum of HCN−Na, corresponding to $\bar{N} = 7200$. To account for the enhanced moment of inertia ($\Delta I_B = 3.23 \times 10^4$ amu·Å^2, $T_{rot} = 0.37$ K), either the equivalent of several hundred helium atoms must rotate rigidly with the dopant about a molecular axis or the dopant must rotate about an axis that is shifted by 26 Å from the HCN−Na center of mass. One possibility, corresponding to the latter scenario, is that the our proposed dopant location is correct and the complex rotates on the surface about an axis through the droplet center of mass. The radius of an *N* helium atom droplet is $R = r_o N^{1/3}$, where $r_o = (4/3\pi\rho)^{-1/3}$ ($\rho = 0.0218$ Å^{-3}), and an $N = 7200$ droplet has a 43 Å radius. Clearly, the agreement between the experiment and this simple model is poor. Nevertheless, as expected for a surface bound dopant rotating about the droplet center, a "particle on a sphere" type *P* and *R* branch spectrum is observed, and the effective moments of inertia depend on both the mass of the dopant and the average droplet radius.

The zero-field spectra were measured for various source conditions, and the size dependence of the rotational constants is shown in Figure 13. The droplet sizes in the figure correspond to the mean size produced at each nozzle source condition without adjusting for the size reduction that occurs upon pick-up and condensation of the dopant. The smooth lines through the data are fits to the functional form (units of MHz)

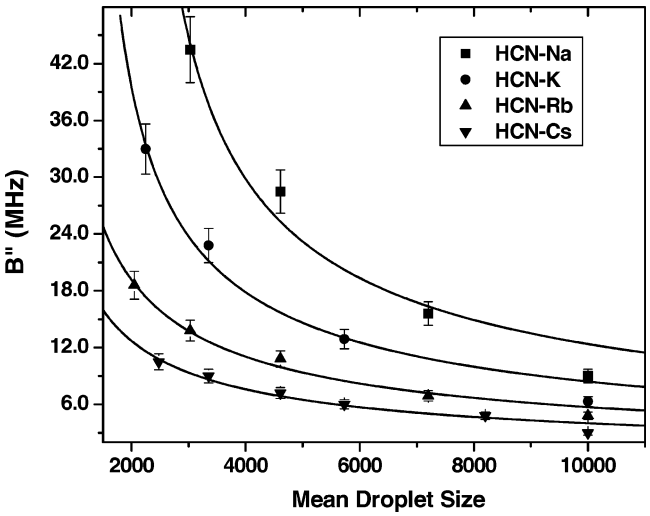

Figure 13. Rotational constants of the HCN−M (M = Na, K, Rb, Cs) complexes as a function of mean droplet size under zero-field conditions. The B'' values were determined with $T_{rot} = 0.37$ K. The smooth curves were obtained by fitting each data set to the functional forms disscused in the text (eqs 2 and 3). The curves for both functional forms overlap such that they are indistinguishable.

$$B(\bar{N}) = \frac{5.0539 \times 10^5}{(M + a)[r_o(\bar{N} - b)^{1/3}]^2} \quad (2)$$

which assumes the complex rotates on the surface about the droplet center of mass. The value of *M* was fixed to the HCN−M mass. The adjustable parameter *b* represents the helium loss upon pick-up and cluster condensation, while the parameter *a* is representative of an additional moment of inertia, resulting from the complex dragging helium density along with it as it moves on the surface. The best fit parameters are given in Table 2.

The fits of each set of data to eq 2 are poor. In particular, the sign of *a* is incorrect, demonstrating that, for *R* values equal to the droplet radius, the effective translational mass of the dopant is predicted to be less than the molecular mass of HCN−M. Lehmann has calculated the hydrodynamic contribution to the HCN−Na effective translational mass in bulk helium to be ∼36 amu, while the value for HCN was determined to be ∼13.5 amu.[69] It is reasonable to expect the hydrodynamic contribution for an HCN−Na complex with HCN solvated and Na on the droplet surface to be between the HCN−Na and the HCN bulk values, leading to values of the *a* parameter between +13.5 and +36 amu. With the effective translational mass ($M + a$) of HCN−Na fixed to 75 amu in eq 2 ($a = 25$ amu), the dopant center of mass is required to be 15−20 Å below the droplet surface. Given the He−HCN−Na intermolecular potential (Figure 2), the predicted location for the dopant center of mass based on the above model is certainly questionable. The energetic cost of solvating the alkali atom is likely too high, and there is no stabilizing term to compensate for the rise in energy. Again, we postulate that the energetically favorable dopant location corresponds to the Na atom residing in a dimple on the surface with the HCN species pointing into the solvent on average toward the droplet center. Nevertheless, this proposed dopant location, which leads to eq 2 as a model for the size dependent rotational constant, is not consistent with the measured B'' values. However, we must note that a tacit

assumption in the above model is that T_{rot} is constant and equal to 0.37 K. Lehmann has demonstrated[70] that the T_{rot} values extracted from high-resolution spectra are biased with respect to the droplet temperature, with T_{rot} being slightly larger than the temperature of the droplet excitations (ripplons).[71,72] Furthermore, the bias grows with the moment of inertia of the solute molecule. Indeed, the moments of inertia of the HCN−M complexes are significantly larger than the values measured for other molecules where T_{rot} could be determined from a resolved rotational spectrum. Consequently, it may be erroneous to assume that $T_{rot} = 0.37$ K in the above model.

Since fitting the unresolved *P* and *R* contours determines only the product of *B* and kT_{rot}, we can estimate the size of the possible bias by fitting the data in Figure 13 to eq 3, with $T_{rot} = 0.37 \times \alpha$ K.

$$B(\bar{N}) = \frac{5.0539 \times 10^5 \times \alpha}{(M + a)[r_o(\bar{N} - b)^{1/3}]^2} \quad (3)$$

Fixing the value of *M* to the mass of HCN−M and that of *a* to 25 amu while adjusting only α and *b*, we obtain the best fit parameters summarized in Table 2. With the addition of the constant scale factor α, the above model fits all of the HCN−M zero-field data well, and all parameters have the correct sign. Therefore, if $T_{rot} = 1.18-1.33$ K, then the measured zero-field HCN−M *B*″ values are compatible with a model consisting of a surface bound dopant rotating about the droplet center of mass. Further theoretical work is required to determine the degree to which the HCN−M T_{rot} values are biased and to corroborate the above model. The origin of this temperature bias is discussed in detail in ref 70.

Upon application of a small (∼200 V/cm) Stark field to the laser interaction region, the HCN−M spectrum changed in two ways that were unexpected. A small ∼50 MHz blue shift of the spectrum occurs in addition to a significant decrease in the overall width of the *P* and *R* branch contours. A smooth transition in the rotational profile is not observed. Instead, each of the HCN−M Stark spectra recorded at 200 V/cm resembles a superposition of two spectra having different products of *B*″ and kT_{rot}. As the Stark field is increased to 500 V/cm, the spectrum with the larger product of *B*″ and kT_{rot} diminishes completely. In the previous section, we assumed throughout that $T_{rot} = 0.37$ K and attributed this change to a Stark field induced enhancement of the effective moment of inertia by approximately 10^4-10^5 amu·Å^2. However, as shown below, the T_{rot} bias cast doubt on this interpretation.

Figure 14 shows the size dependence of the HCN−Na and HCN−K rotational constants extracted from the 500 V/cm Stark spectra. In contrast to the zero-field case, the variation of the 500 V/cm rotational constants fits very well to eq 2 when T_{rot} is fixed to 0.37 K. The fits are shown as smooth curves in Figure 14. The best fit parameters are given in Table 2, showing *a* values of 15 and 24 amu for M = Na and K, respectively. The additional α scale factor is not required for a satisfactory fit. If however, we fix *a* = 25 amu, as we did for the zero-field data, α values close to 1.0 (summarized in Table 2) are obtained for both M = Na and M = K.

If the center of mass of the HCN−M complex is on the surface of the droplet, then the moment of inertia should scale linearly with the mass of HCN−M for a fixed mean droplet size. A linear fit to the HCN−M moments of inertia measured at 500 V/cm is shown in Figure 15. All of the data points correspond to measurements at a fixed mean droplet size of approximately $\bar{N} = 7200$, and the I_B values are determined with

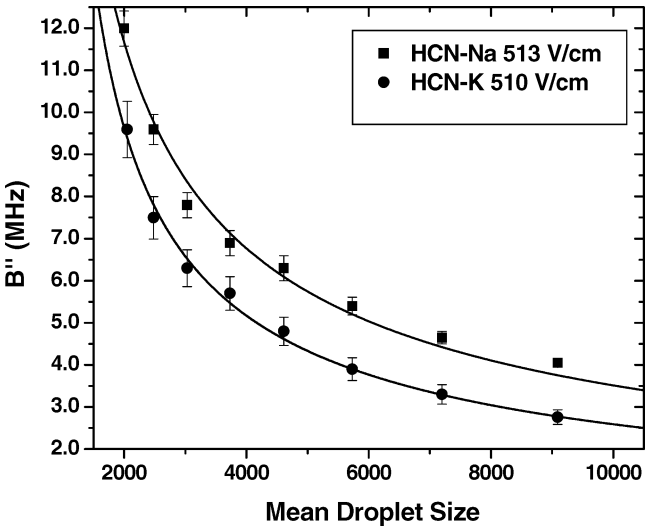

Figure 14. Rotational constants of the HCN−Na and HCN−K complexes as a function of the mean droplet size. The rotational constants were obtained from simulations of the ∼510 V/cm Stark spectra recorded at various nozzle temperatures. The *B*″ values were determined with $T_{rot} = 0.37$ K. The smooth curves were obtained by fitting each data set to the functional forms disscused in the text (eqs 2 and 3). The curves for both functional forms overlap such that they are indistinguishable.

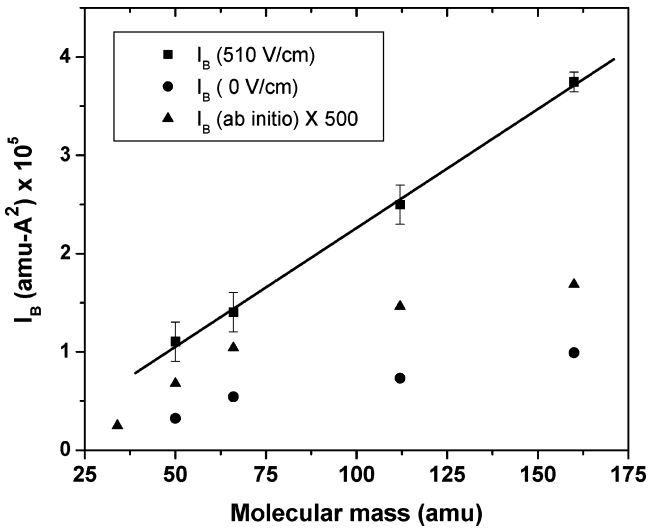

Figure 15. Moments of inertia for the HCN−M (M = Na, K, Rb, Cs) complexes as a function of the complex mass under Stark field conditions (∼510 V/cm, $T_{rot} = 0.37$K; squares). The mean droplet size was fixed to approximately 7200 helium atoms by keeping the nozzle temperature at 18.0 K for all four complexes. The linear fit corresponds to an *R* value of 0.9991. Also shown are the moments of inertia for the HCN−M complexes under zero-field conditions for the same mean droplet size (circles), along with the ab initio values (triangles) multiplied by a factor of 500.

$T_{rot} = 0.37$ K. Indeed, the moment of inertia increases linearly as the mass of the dopant increases. Since $I = MR^2$, the square root of the slope of the line gives an average droplet radius, $\bar{R} = 49 \pm 1$Å. Averaging $R = r_o N^{1/3}$ over the 60 bar, 18.0 K statistical distribution of droplet sizes containing exactly one HCN and one M atom, we obtain an average radius of 46 Å, in good agreement with the value obtained from the fit. Certainly, with the assumption that $T_{rot} = 0.37$ K, the size and mass dependence of the 500 V/cm *B*″ values is consistent with a model in which the dopant is rotating on the surface about the center of the droplet. Without having to consider a bias in T_{rot},

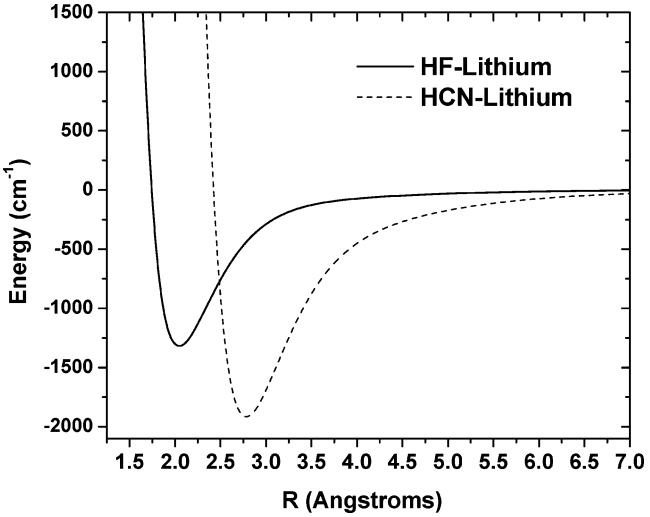

Figure 16. Comparison of 1D cuts of the HCN−Li and HF−Li potential energy surfaces. The potentials (RMP2/aug-cc-pVTZ) are counterpoise corrected. The value of the other Jacobi coordinate, θ, was constrained to 180 and 120 degrees for HCN−Li and HF−Li, respectively. HCN−Li has the more attractive potential at long range ($R \geq 5$Å).

the value of R, determining the moment of inertia of the rotational motion, is simply the average droplet radius.

The results reported here clearly show that, for HCN−M complexes embedded in helium droplets, the product of B'' and kT_{rot} decreases by approximately a factor of 3.5 upon application of the Stark field. However, further theoretical work will be required to determine the origin of this effect. If B'' is the same for both the zero-field and the Stark spectra and the broader zero-field rotational profiles are due to a bias in T_{rot}, then it is not clear to us why the bias is removed upon application of the 500 V/cm Stark field. Moreover, if on the other hand T_{rot} is the same for both zero-field and Stark conditions, then the Stark induced change in B'' corresponds to a significant change in the solvation environment of the dopant. This change corresponds to the dopant center of mass being forced toward the droplet surface from ∼15−20 Å below. Given the above energetic argument for the dopant location, a partially solvated dopant with the Stark field off is not likely. Additionally, this conjecture is unphysical, since the Stark energy for HCN−M in a 500 V/cm Stark field is 0.06 cm^{-1}, which should be compared with $kT = 0.26$ cm^{-1} and the HCN−M solvation energy, which is on the order of 100 cm^{-1}.[73] Hence, it does not appear reasonable that an external Stark field of this magnitude could induce a large change in the dopant solvation environment.

One objection to the above model is that the complex may not be capable of undergoing free rotation on the surface because of the coupling of this motion to the surface ripplon modes. Neverthess, the coupling of the rotational motion of the dopant to the ripplons and hence the relaxation time scale for this motion are unknown. Certainly, future theoretical work is required to validate the above model in which the HCN−M complex, exhibiting a large bias in T_{rot}, rotates on the surface about the droplet center.

Finally, we would like to point out that, despite many attempts, we were unable to obtain spectra for the hydrogen fluoride (HF)−alkali atom complexes. This was surprising, given that we also observed complexes of Na and K with cyanoacetylene (HCCCN). In addition, the ab initio calculations suggested that the complexes were all strongly bound with binding energies ≥800 cm^{-1}. Therefore, it is not clear why we were unable to observe the spectra of the HF−M complexes, which are predicted to have strong absorptions in the 2−3 μm region of the infrared. It is reasonable to suspect that the long-range interactions between the two subunits are important in determining the probability of forming the complex, since complexation may rely on the HCN or HF molecule being attracted to the atom on the droplet surface. Figure 16 shows 1D slices of the RMP2 HCN−Li and HF−Li potential surfaces, illustrating the difference in the long range interactions. The HCN−Li interaction is more attractive at long-range, resulting from the larger dipole−induced dipole interaction for the more polar HCN molecule. As a result, the HCN fragment is not required to approach as closely before being steered toward complex formation. In comparison, if the droplet potential keeps the HF molecule from approaching within 4 Å of the Li atom, the complex may never form. We propose that the majority of HF molecules picked up by the droplets will not come close enough to the alkali atom to form the complex, accounting for the absence of complexes in the HF−M infrared spectra.

6. Summary

The binary complexes of HCN−M (M = Na, K, Rb, and Cs) were formed on the surface of helium droplets by a sequential pick-up of the alkali atom followed by the HCN molecule. When fitted to a linear rotor Hamiltonian, the infrared spectrum of the ν_1 fundamental CH stretch band revealed an extreme enhancement of the moment of inertia on the order of 10^4-10^5 amu·Å^2. The effective moment of inertia was found to be strongly dependent on both the average droplet size and the mass of the dopant. A model for the rotational dynamics was proposed to account for the dopant mass and droplet size dependence of $I_{0V/cm}$. In the model, the alkali atom of the complex is located in a dimple site on the surface of the droplet. The HCN end of the HCN−M complex is solvated in the liquid, with the permanent dipole moment oriented on average parallel to the vector connecting the droplet and the dopant centers of mass. The dopant rotates on the surface about the center of the droplet with a characteristic rotational temperature significantly biased with respect to the droplet temperature. The application of a 500 V/cm Stark field to the laser interaction region changes the overall width of the P and R contours such that the product of B'' and kT_{rot} is reduced by a factor of 3.5. Given the droplet size and dopant mass dependence of $I_{510V/cm}$, the modest Stark field apparently provides a mechanism to turn off the apparent temperature bias observed for the zero-field condition. However, the origin of this effect is currently undetermined.

Acknowledgment. This work was supported by the National Science Foundation (Grant CHE-99-87740). G.D. would like to acknowledge the Graduate School at UNC-CH for a Royster Fellowship. G.D. also acknowledges Carlo Callegari for initially suggesting to us the surface bound location of the HCN-Na complex and for his encouragement to carry out the droplet size dependent study presented here. Kevin Lehmann is also gratefully acknowledged for his helpful suggestions throughout the course of this work and during the preparation of the manuscript.

Supporting Information Available: He-HCN-Na potential energy surface; HCN−NA potential, HCN/HF−Li potential, and Na−He potential. This material is available free of charge via the Internet at http://pubs.acs.org.

Note Added after ASAP Publication. This article was released ASAP on June 29, 2007. Some minor typographical changes have occurred in paragraphs 4 and 5 of the Introduction section. The corrected version posted on July 2, 2007.

References and Notes

(1) Kinoshita, T.; Fukuda, K.; Matsuura, T.; Yabuzaki, T. *Phys. Rev. A* **1996**, *53*, 4054−4063.

(2) Takahashi, Y.; Sano, K.; Kinoshita, T.; Yabuzaki, T. *Phys. Rev. Lett.* **1993**, *71*, 1035−1038.

(3) Fujisaki, A.; Sano, K.; Kinoshita, T.; Takahashi, Y.; Yabuzaki, T. *Phys. Rev. Lett.* **1993**, *71*, 1039−1042.

(4) Goyal, S.; Schutt, D. L.; Scoles, G. *Phys. Rev. Lett.* **1992**, 69, 933−936.

(5) Frochtenicht, R.; Toennies, J. P.; Vilesov, A. F. *Chem. Phys. Lett.* **1994**, *229*, 1−7.

(6) Hartmann, M.; Miller, R. E.; Toennies, J. P.; Vilesov, A. F. *Phys. Rev. Lett.* **1995**, *75*, 1566−1569.

(7) Stienkemeier, F.; Ernst, W. E.; Higgins, J.; Scoles, G. *J. Chem. Phys.* **1995**, *102*, 615−617.

(8) Lewerenz, M.; Schilling, B.; Toennies, J. P. *J. Chem. Phys.* **1995**, *102*, 8191−8207.

(9) Lewerenz, M.; Schilling, B.; Toennies, J. P. *J. Chem. Phys.* **1997**, *106*, 5787−5787.

(10) Stienkemeier, F.; Higgins, J.; Ernst, W. E.; Scoles, G. *Phys. Rev. Lett.* **1995**, *74*, 3592−3595.

(11) Stienkemeier, F.; Higgins, J.; Ernst, W. E.; Scoles, G. *Z. Phys. B* **1995**, *98*, 413−416.

(12) Stienkemeier, F.; Higgins, J.; Callegari, C.; Kanorsky, S. I.; Ernst, W. E.; Scoles, G. *Z. Phys. D* **1996**, *38*, 253−263.

(13) Reho, J.; Higgins, J.; Callegari, C.; Lehmann, K. K.; Scoles, G. *J. Chem. Phys.* **2000**, *113*, 9686−9693.

(14) Reho, J.; Callegari, C.; Higgins, J.; Ernst, W. E.; Lehmann, K. K.; Scoles, G. *Faraday Discuss.* **1997**, *108*, 161−174.

(15) Bruhl, F. R.; Trasca, R. A.; Ernst, W. E. *J. Chem. Phys.* **2001**, *115* (22), 10220−10224.

(16) Dropplemann, G.; Bunermann, O.; Schulz, C. P.; Stienkemeier, F. *Phys. Rev. Lett.* **2004**, *93*, 023402.

(17) Bunermann, O.; Mudrich, M.; Weidemuller, M.; Stienkemeier, F. *J. Chem. Phys.* **2004**, *121*, 8880−8886.

(18) Nakayama, A.; Yamshita, K. *J. Chem. Phys.* **2001**, *114*, 780−791.

(19) Stienkemeier, F.; Bunermann, O.; Mayol, R.; Ancilotto, F.; Barranco, M.; Pi, M. *Phys. Rev. B* **2004**, *70*, 214508.

(20) Reho, J.; Higgins, J.; Scoles, G. *J. Chem. Phys.* **2000**, *113*, 9694−9701.

(21) Stienkemeier, F.; Meier, F.; Hagele, A.; Lutz, H. O. *Phys. Rev. Lett.* **1999**, *83*, 2320−2323.

(22) Vongehr, S.; Scheidemann, A. A.; Wittig, C.; Kresin, V. V. *Chem. Phys. Lett.* **2002**, *353*, 89−94.

(23) Rice, B. M.; Grosh, J.; Thompson, D. L. *J. Chem. Phys.* **1995**, *102*, 8790−8799.

(24) Higgins, J.; Callegari, C.; Reho, J.; Stienkemeier, F.; Ernst, W. E.; Gutowski, M.; Scoles, G. *J. Phys. Chem. A* **1998**, *102*, 4952−4965.

(25) Reho, J. H.; Higgins, J. P.; Lehmann, K. K. *Faraday Discuss.* **2001**, *118*, 33−42.

(26) Mudrich, M.; Bunermann, O.; Stienkemeier, F.; Dulieu, O.; Weidemuller, M. *Eur. Phys. J. D* **2004**, *31*, 291−299.

(27) Bruhl, F. R.; Miron, R. A.; Ernst, W. E. *J. Chem. Phys.* **2001**, *115*, 10275−10281.

(28) Higgins, J.; Ernst, W. E.; Callegari, C.; Reho, J.; Lehmann, K. K.; Scoles, G.; Gutowski, M. *Phys. Rev. Lett.* **1996**, *77*, 4532−4535.

(29) Higgins, J.; Callegari, C.; Reho, J.; Stienkemeier, F.; Ernst, W. E.; Lehmann, K. K.; Gutowski, M.; Scoles, G. *Science* **1996**, *273*, 629−631.

(30) Reho, J. H.; Higgins, J.; Nooijen, M.; Lehmann, K. K.; Scoles, G.; Gutowski, M. *J. Chem. Phys.* **2001**, *115*, 10265−10274.

(31) Schulz, C. P.; Claas, P.; Schumacher, D.; Stienkemeier, F. *Phys. Rev. Lett.* **2004**, *92*, 013401.

(32) Patil, S. H. *J. Chem. Phys.* **1991**, *94*, 8089−8099.

(33) Scoles, G. *Int. J. Quant. Chem.* **1990**, *24*, 475−479.

(34) Dalfovo, F. *Z. Phys. D* **1994**, *29*, 61−74.

(35) Ancilotto, F.; Lerner, P. B.; Cole, M. W. *J. Low Temp. Phys.* **1995**, *101*, 1123−1146.

(36) Hartmann, M.; Portner, N.; Sartakov, B.; Toennies, J. P.; Vilesov, A. F. *J. Chem. Phys.* **1999**, *110*, 5109−5123.

(37) Nauta, K.; Miller, R. E. *Phys. Rev. Lett.* **1999**, *82*, 4480−4483.

(38) Lugovoj, E.; Toennies, J. P.; Vilesov, A. F. *J. Chem. Phys.* **2000**, *112*, 8217−8220.

(39) Lovallo, C. C.; Klobukowski, M. *Chem. Phys. Lett.* **2003**, *373*, 439−447.

(40) Chang, X. Y.; Ehlich, R.; Hudson, A. J.; Piecuch, P.; Polanyi, J. C. *Faraday Discuss.* **1997**, *108*, 411−425.

(41) Topaler, M. S.; Truhlar, D. G.; Chang, X. Y.; Piecuch, P.; Polanyi, J. C. *J. Chem. Phys.* **1998**, *108*, 5349−5377.

(42) Topaler, M. S.; Truhlar, D. G.; Chang, X. Y.; Piecuch, P.; Polanyi, J. C. J. *Chem. Phys.* **1998**, *108*, 5378−5390.

(43) Zeiri, Y.; Katz, G.; Kosloff, R.; Topaler, M. S.; Truhlar, D. G.; Polanyi, J. C. *Chem. Phys. Lett.* **1999**, *300*, 523−528.

(44) Hudson, A. J.; Oh, H. B.; Polanyi, J. C.; Piecuch, P. *J. Chem. Phys.* **2000**, *113*, 9897−9900.

(45) Dobrin, S.; Giorgi, J. B.; Naumkin, F. Y.; Polanyi, J. C. *J. Chem. Phys.* **2005**, *122*, 014705.

(46) Kasai, P. H. *J. Am. Chem. Soc.* **1998**, *120*, 7884−7892.

(47) Kasai, P. H. *J. Phys. Chem. A* **2000**, *104*, 4514−4520.

(48) Choi, M. Y.; Douberly, G. E.; Falconer, T. M.; Lewis, W. K.; Lindsay, C. M.; Merritt, J. M.; Stiles, P. L.; Miller, R. E. *Int. Rev. Phys. Chem.* **2006**, *25*, 15−75.

(49) Knuth, E. L.; Schilling, B.; Toennies, J. P. *International Symposion on Rarefied Gas Dynamics;* Oxford University Press: Oxford, U.K., 1995; Vol. 19, pp 270−276.

(50) Stiles, P. L.; Moore, D. T.; Miller, R. E. *J. Chem. Phys.* **2003**, *118*, 7873−7881.

(51) Stiles, P. L.; Moore, D. T.; Miller, R. E. *J. Chem. Phys.* **2004**, *121*, 3130−3142.

(52) Nauta, K.; Moore, D. T.; Stiles, P. L.; Miller, R. E. *Science* **2001**, *292*, 481−484.

(53) Reho, J.; Merker, U.; Radcliff, M. R.; Lehmann, K. K.; Scoles, G. *J. Chem. Phys.* **2000**, *112*, 8409−8416.

(54) Veeco Learning Center. http://www.veeco.com (accessed Aug 2005).

(55) Huang, Z. S.; Jucks, K. W.; Miller, R. E. *J. Chem. Phys.* **1986**, 85, 3338−3341.

(56) Werner, H. J.; Knowles, P. J.; Almlof, J.; Amos, R. D.; Berning, A.; Deegan, M. J. O.; Eckert, F.; Elbert, S. T.; Hampel, C.; Lindh, R.; Meyer, W.; Nicklass, A.; Peterson, K.; Pitzer, R.; Stone, A. J.; Taylor, P. R.; Mura, M. E.; Pulay, P.; Scheutz, M.; Stoll, H.; Thorsteinsson, T.; Cooper, D. L. *MOLPRO version 2002.1*; Cardiff University: Cardiff, U.K., 2002.

(57) Dolg, M.; Stoll, H.; Preuss, H.; Pitzer, R. M. *J. Phys. Chem.* **1993**, *97*, 5852−5859.

(58) Fuentealba, P.; Preuss, H.; Stoll, H.; von Szentpaly, L. *Chem. Phys. Lett.* **1982**, *89*, 418−422.

(59) Boys, S. F.; Bernardi, F. *Mol. Phys.* **1970**, *19*, 553−566.

(60) Rost, J. M.; Griffin, J. C.; Friedrich, B.; Herschbach, D. R. *Phys. Rev. Lett.* **1992**, *68*, 1299−1301.

(61) Nauta, K.; Moore, D. T.; Miller, R. E. *Faraday Discuss.* **1999**, *113*, 261−278.

(62) Nauta, K.; Miller, R. E. *Science* **1999**, *283*, 1895−1897.

(63) Mayol, R.; Ancilotto, F.; Barranco, M.; Bunermann, O.; Pi, M.; Stienkemeier, F. *J. Low Temp. Phys.* **2005**, *138*, 229−234.

(64) Merritt, J. M.; Douberly, G. E.; Miller, R. E. *J. Chem. Phys.* **2004**, *121*, 1309−1316.

(65) Kwon, Y.; Whaley, K. B. *Phys. Rev. Lett.* **1999**, *83*, 4108−4111.

(66) Moroni, S.; Blinov, N.; Roy, P. *J. Chem. Phys.* **2004**, *121*, 3577−3581.

(67) Maroni, S.; Sarsa, A.; Fantoni, S.; Schmidt, K. E.; Baroni, S. *Phys. Rev. Lett.* **2003**, *90*, 143401.

(68) Lehmann, K. K. *Mol. Phys.* **1999**, *97*, 645−666.

(69) Lehmann, K. K. private communication, 2005.

(70) Lehmann, K. K. *J. Chem. Phys.* **2004**, *120*, 513−515.

(71) Lehmann, K. K. *J. Chem. Phys.* **2003**, *119*, 3336−3342.

(72) Lehmann, K. K.; Dokter, A. M. *Phys. Rev. Lett.* **2004**, *91*, 173401.

(73) Schmied, R.; Lehmann, K. K. unpublished result.